



## Thermobaric effects formed by aluminum foils enveloping cylindrical charges



Qi-Long Yan<sup>a</sup>, Waldemar A. Trzciński<sup>b</sup>, Stanisław Cudziło<sup>b,\*</sup>, Józef Paszula<sup>b</sup>, Trană Eugen<sup>c</sup>, Mătache Liviu<sup>d</sup>, Rotariu Traian<sup>c,\*</sup>, Michael Gozin<sup>a,\*</sup>

<sup>a</sup> School of Chemistry, Faculty of Exact Sciences, Tel Aviv University, Tel Aviv 69978, Israel

<sup>b</sup> Institute of Chemistry, Military University of Technology, Kaliskiego 2, PL-00 908 Warsaw, Poland

<sup>c</sup> Military Technical Academy, Bucharest 050141, Romania

<sup>d</sup> Scientific Research Center for CBRN Defense and Ecology, 225 Sos. Oltenitei, 041309 Bucharest, Romania

### ARTICLE INFO

#### Article history:

Received 5 November 2015

Revised 12 January 2016

Accepted 12 January 2016

Available online 18 February 2016

#### Keywords:

Detonation

Combustion

Explosives

Thermobaric

Al foil

### ABSTRACT

Conceptually new cylindrical charges enveloped by Al foils have been designed and their thermobaric effects, due to simultaneous fragmentation and combustion of the foils, have been experimentally determined. The fragmentation processes of Al foil was supported by numerical simulations. It has been shown that the quasistatic pressures (QSP) for phlegmatized RDX ( $\text{RDX}_{\text{ph}}$ ) enveloped with Al-coated plastic foils are higher than that of the pure  $\text{RDX}_{\text{ph}}$ , due to combustion of these foil fragments in a thermobaric explosion. The QSP generated by Al–Ni foils enveloping  $\text{RDX}_{\text{ph}}$  was found to be much lower than performance of other foils, possibly due to relatively inert nature of Ni. In a small detonation chamber, the charges of  $\text{RDX}_{\text{ph}}$ /Al foil ( $\text{RDX}_{\text{ph}}$ /Alf) produced even higher experimental maximum peak pressure ( $\Delta p_{\text{max}}$ ) than the charges that contained Al powder ( $\text{Al}_p$ ). In a closed bunker, the impulse amplitudes of  $\text{RDX}_{\text{ph}}$  enveloped by aluminized polyethylene (Al-PE) foils and  $\text{RDX}_{\text{ph}}$  enveloped by 100  $\mu\text{m}$  Alf (Alf100) charges are much lower than those of the other charges. It was found that the charges enveloped by Al foils have even larger  $\Delta p_{\text{max}}$  than that of  $\text{RDX}_{\text{ph}}$ /Al<sub>p</sub> charges, indicating that the Alf could generate better blast performances than the Al<sub>p</sub>. The simulations indicate that the observed blast enhancement is dependent not on the thickness, but on the size of surrounding space. The thermobaric fire-ball generated by 40 g  $\text{RDX}/\text{Alf}$  charge could sustain combustion up to 40 ms, reaching a maximum radius of about 2.4 m.

© 2016 The Combustion Institute. Published by Elsevier Inc. All rights reserved.

### 1. Introduction

Thermobaric explosives (TBXs), also regarded as solid fuel-air explosives (SFAE), over the years have created a great interest since they are highly destructive in enclosed spaces such as underground constructions, tunnels, and field fortifications [1–4]. Thermobaric effects refer to heat and pressure effects, instead of armor penetrating or fragmentation damage effects [5]. In TBX formulations, a large proportion of metal fuels are usually used to generate the heat in a secondary combustion after the detonation of the main charge. In particular, Al is the most widely used metal for this purpose [6]. Due to its high ignition temperature ( $T_i$ ) and partial inertness during detonation, the optimum amount of Al might differ, depending on the type and content of the explosive fillers in TBXs. However, the efficient use of Al in energetic compositions including TBXs remains challenging due to several reasons.

One such example is the use of micrometer-sized Al that may agglomerate, resulting in lower combustion efficiency and increased two-phase flow losses [7]. The use of nano-sized Al (nAl) may improve the combustion performance and reduce the particle size of the final agglomerated products, but it would reduce the energy release due to a higher inert  $\text{Al}_2\text{O}_3$  content. Moreover, a very high surface area (10–50  $\text{m}^2 \text{g}^{-1}$ ) of nAl particles can lead to rheological problems during processing (e.g. difficulty in casting) [8]. The combination of nAl (e.g. 75 nm) and coarse Al (e.g. 250  $\mu\text{m}$ ) particles with equal fractions may partially solve these problems [9].

In order to improve the heat releases and combustion efficiency of nAl in both propellants and TBXs, many strategies have been developed. For instance, energetic blends of nAl particles with liquid perfluorocarbon-based oxidizers, such as perfluoropolyethers (PFPE) were prepared. In this way, exothermic reaction on the surface between fluorine and the  $\text{Al}_2\text{O}_3$  shell could be activated, and hence the reactivity of nAl particle is improved, leading to a significant increase in the flame speed. It has been proved that the oxygen and fluorine have equal probability to react with Al [10,11]. In addition, the ignitability of the Al/ polytetrafluoroethylene

\* Corresponding authors.

E-mail address: [cogozin@gmail.com](mailto:cogozin@gmail.com) (M. Gozin).

(Al/PTFE) composite can be improved by mechanical activation such as milling. The activated samples can be readily ignited by using a butane flame, while the physical mixtures of micro-sized Al and PTFE are only ignitable with an exposure to continuous flame [12]. Another facile way of promoting the reactivity of Al<sub>p</sub> is to introduce a liquid perfluorinated or fluoro-oligomer by physisorption on the surface of Al<sub>p</sub> [13,14]. When fluorine replaces oxygen as the oxidizing agent, AlF<sub>3</sub> is formed instead of Al<sub>2</sub>O<sub>3</sub>, both of which are thermodynamically stable with heats of formation of 1510 and 1676 kJ mol<sup>-1</sup>, respectively [15]. In addition to fluoropolymer, the activation of Al<sub>p</sub> could also be achieved by combining with the other metals. For instance, the equiatomic Al–Ni mixtures after milling can reduce exothermic onset of Al<sub>p</sub> by as much as 300 °C [16]. The use of Al–Ni composite in a solid propellant could reduce the agglomeration of Al<sub>p</sub> and decrease its ignition delay.

Generally, two major issues may affect the performances of aluminized TBXs. The rule is that there must be sufficient energy from the primary detonation for achieving the  $T_i$  of the Al, while the entire charge should be oxygen-deficient. As mentioned above, the particle size of Al and the surface coating may influence the  $T_i$  of Al, and lowering the  $T_i$  of Al particles can increase the performances of TBXs [17]. In order to fulfill the above-mentioned requirements, the charge designs in terms of compositions and structures are equally important. Recently, several novel oxygen-deficient compositions have been developed, which contains a reactive metal, binder, and plasticizer, sometimes with addition of a catalyst [18]. Moreover, a class of charges using an annular design was developed, where a cylindrical shell of a metalized charge surrounds the high explosive charge [19]. A recent study by Trzciński and coworkers regarding the explosion of an annular charge showed the improved performance as a TBX charge [20–23]. It was composed of a phlegmatized RDX (RDX<sub>ph</sub>) core and a layer of ammonium nitrate (AN)/Al particles mixture. The influence of Al contents and particle sizes on a quasi-static pressure (QSP) of explosion was further studied by the same group [24]. In fact, the core explosive charge may generate enough energy to break the out-layer metals and simultaneously ignite the fragmented metal particles in surrounding air. It was further found that, even a significant mass of the steel case of an explosive charge can be burned to enhance air blast in the chamber [25]. In this work, a conceptually new design of TBX was developed and tested. In this new design, the Al powder inside the conventional TBX charges was removed, and replaced by enveloping the core charge with Al foils. The general idea behind this design was that upon detonation, the layers of Al foil would be fragmented into micron-sized particles, and subsequently ignited in the air, generating thermobaric effect. The Al foils are simply made of pure Al or activated aluminized composites containing polymers or Ni foil as mentioned above, in order to decrease the  $T_i$  of the Al. The experiments in this work were conducted in both open field and confined spaces (including 0.15 and 40 m<sup>3</sup> chambers). In addition to straightforward preparation of newly designed TBXs from the commercially available Al foils and aluminized plastic films, their performances have been tested by various experimental techniques. The observed performances of these new charges showed the significant advantages of previously known designs.

## 2. Experiments and theory

### 2.1. Charge compositions and quasi-static pressure measurements

The cylindrical charges used in QSP tests had an explosive core with a diameter of 20.0 mm. It was composed of two pellets of RDX/wax 94/6 composition (RDX<sub>ph</sub>). The pellets had a density of 1.66 g cm<sup>-3</sup> and were glued together. The mass of RDX<sub>ph</sub> cores was 25.0 g. The external layer (envelope) included of Al foil (Alf), Al

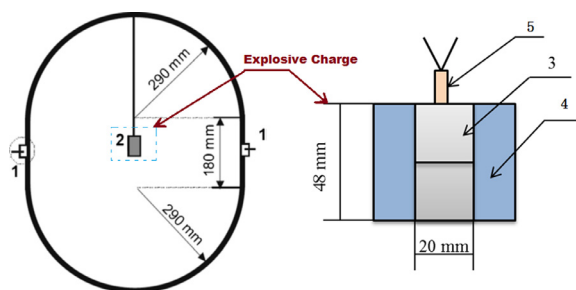


Fig. 1. Schematic of the investigated layered charge and the 0.15-m<sup>3</sup> explosion chamber (side view): 1 – pressure gauges, 2 – explosive charge, 3 – RDX<sub>ph</sub> (25 g), 4 – envelope (40 g), 5 – fuse.

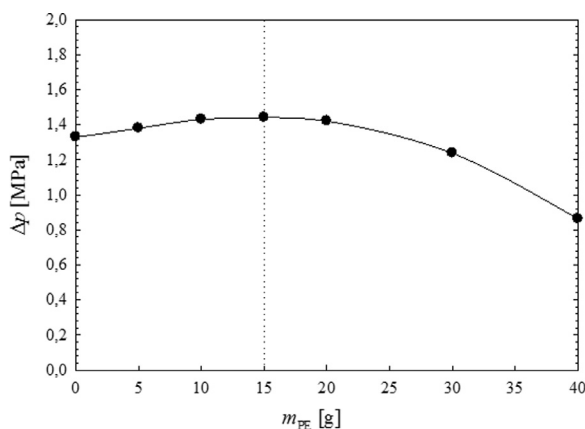


Fig. 2. Dependence of overpressure in the 0.15-m<sup>3</sup> chamber on the mass of PE foil in the Al/PE envelope.

Table 1

Compositions of the charges for QSP tests.

Charge symbol	Mass of the component [g]					
	RDX <sub>ph</sub>	Alf	PTFE	Ni	PE	Alp
RDX <sub>ph</sub>	25.0	–	–	–	–	–
RDX <sub>ph</sub> +Al foil (Alf)	25.0	40.0	–	–	–	–
RDX <sub>ph</sub> +Al/PTFE foils	25.0	10.0	30.0	–	–	–
RDX <sub>ph</sub> +Al/Ni foils	25.0	23.8	–	16.2	–	–
RDX <sub>ph</sub> +Al/PE foils	25.0	25.0	–	–	15.0	–
RDX <sub>ph</sub> +Al powder	25.0	–	–	–	–	40.0

powder (Al<sub>p</sub>) or combinations of Al/PTFE, Al and polyethylene foils (Al/PE), Al and nickel foils (Al/Ni). The mass of the external layer (envelope) was 40 g, which were wound alternately and uniformly in the case of two component layers. Figure 1 shows a cross section of an explosion chamber and cylindrical layered charge applied in the tests.

The thickness of Al was 10 or 100 μm, while the PTFE, PE and Ni foils were 200, 100 and 125 μm, respectively. Mass ratio of Al/PTFE and Al/Ni out-layers corresponded to the stoichiometry of the following reactions: 3C<sub>2</sub>F<sub>4</sub>+4Al=4AlF<sub>3</sub>+6C and 3Al+Ni=NiAl<sub>3</sub>. In the case of Al/PE envelope, mass fraction of PE and Al foils was determined using CEETAH code [26]. The calculated overpressure in a 0.15-m<sup>3</sup> chamber filled with air after detonation of a charge containing 15 g PE and 25 g Al had the maximal value of approx. 1.4 MPa, Fig. 2.

The purity of Al<sub>p</sub> used in the experiments was above 99.5%, and its particle diameters were below 44 μm (325 mesh). The powder was placed in a thin-walled paper tube of 38 mm in diameter, surrounding the RDX<sub>ph</sub> core (Table 1).

QSP tests were performed in a chamber of about 0.15 m<sup>3</sup> volume, which was filled with air at pressure of 0.1 MPa. The

ambient temperature was 18 °C. A charge was hung in the center of the chamber. A standard electrical detonator (fuse) was applied to initiate the RDX<sub>ph</sub> charge. A mass of 1.3 g of PETN can be assumed as an energetic equivalent of the explosive and firing composition of the detonator. Signals of overpressure (reflected waves) from two piezoelectric gauges (M102A or M102A03 from PCB Piezotronics, Inc.) located at the chamber's wall were recorded by a digital storage scope (Fig. 1). To reduce the vibrations from the chamber a Teflon sheet separating the chamber body from the transducer was applied. The transducers were also protected from the damage of hot gases by a layer of black electrical tape. The pressure histories measured in the explosion chamber were fitted by using the following Eq. (1).

$$\Delta p_{\text{appr}} = a(1 - e^{-bt}) + ce^{-dt} \quad (1)$$

where  $a$ ,  $b$ ,  $c$  and  $d$  are constants. The first part describes the growth of the average pressure in the chamber due to combustion of Al particles in the air and detonation products, the second one is responsible for the pressure drop caused by the transmission of heat from the gaseous medium to the steel wall of the chamber. Eq. (1) reaches a maximum  $\Delta p_{\text{max}}$  at the time  $t_{\text{max}}$ , described as Eq. (2).

$$t_{\text{max}} = \ln\left(\frac{ab}{cd}\right) \frac{1}{b-d} \quad (2)$$

## 2.2. Evaluation of the Alf fragmentation

As a well-known fact, the energy released on detonation of high explosive charges enclosed in metallic shell usually generates fragmentation and high velocity shrapnel [27–29]. Over the time, the complex phenomenon of metallic shell fragmentation has been approached by many researchers like Rosin and Rammler [30], Lineau [31], Weibull [32], Schuhmann [33], Mott [27], Gilvary [34], Shockey [35], and Grady [28]. From the previously-mentioned models, only two have been widely used: statistical-physical-model (Mott model) and energy-based model (Grady model). Both Mott and Grady models were built mainly for describing the fragmentation of bulk ductile metallic cases during high explosive charge detonation. Given that Al is also a ductile metal (even for thin foils), an evaluation of Al foil envelope fragmentation was investigated based on Mott and Grady assumptions. However, since at high temperature and pressure, the Al is a reactive metal, the fragmentation evaluation will be focused on determination of the characteristic fragment lengths and its distribution. In fact, since this approach was quite justified, as previously pointed out by Zhang [36], for the shell surrounding an explosive charge, only the small fragments could lead to a high rate of energy release. According to Mott theory, the characteristic fragment lengths and their distribution can be evaluated by means of the following expressions [27]:

$$l_0 = 1.5 \sqrt{\frac{2P_F}{\rho 160 \frac{P_2}{P_F(1+S_F)} \dot{\epsilon}^2}} \quad (3)$$

$$N(> l) = N_T e^{-\left(\frac{l}{l_0}\right)^{1/2}} \quad (4)$$

where  $P_F$  and  $S_F$  are true fracture stress and strain;  $P_2$  is the proportionality coefficient in the strain-hardening law for the material at high strains  $P = P_1 + P_2 \ln(1 + S_F)$ ;  $\rho$  represents the material density;  $N(> l)$  is the cumulative number of fragments with a length exceeding  $l$ ,  $N_T$  represents the total number of fragments, and  $l_0$  stands for the average fragment length. As for Grady approach, the nominal fragment width and the corresponding distribution are

evaluated through [28]:

$$\lambda = \left(\frac{48\Gamma}{\rho \dot{\epsilon}^2}\right)^{1/3} \quad (5)$$

$$\Gamma = \frac{K_c^2}{2\rho c^2} \quad (6)$$

$$N(> l) = N_T e^{-\frac{l}{\lambda}} \quad (7)$$

where  $\lambda$  is the average fragment length,  $\Gamma$  stands for fracture surface energy per unit area,  $\dot{\epsilon}$  represents the circumferential strain rate,  $c$  denotes the sound speed in the material and  $K_c$  is the dynamic fracture toughness. As can be easily seen in the above expressions, the envelope thickness is not a distinctive input parameter. More recently, Goloveshkin and Myakov [37] put forth a slightly different approach, in which the average fragments length (Eq. (8)) and the average fragment number (Eq. (9)) are expressed as a function of the envelope thickness. Since no distribution law has been mentioned for this particular model, a power one expression will be considered:

$$2a = \left(\frac{16\sqrt{3}Yh}{\rho \dot{\epsilon}^2}\right)^{1/3} \quad (8)$$

$$N_T = \pi R \left(\frac{\rho \dot{\epsilon}^2}{2\sqrt{3}Yh}\right)^{1/3} \quad (9)$$

$$N(> l) = N_T e^{-\frac{l}{2a}} \quad (10)$$

where  $Y$  is the yield stress,  $h$  for the half of thickness and  $R$  the shell radius.

## 2.3. Pressure histories in a large bunker

The experiments with larger charges were performed in the bunker which schematic and the locations of a charge and gauges are shown in Fig. S1 (Supporting information). The bunker has a volume of about 40 m<sup>3</sup>, and it has four small openings each with a surface of 0.05 m<sup>2</sup> and a frontage opening with a surface about 1.3 m<sup>2</sup>. Tested charge was placed 1.5 m above the ground in the bunker. The blast pressure history was measured by piezoelectric four gauges (137A21 or 137A22 from PCB Piezotronics, Inc.) fixed at distances of 2 m (two gauges) and 2.5 m (two gauges) from the charge. All gauges recorded the overpressure of an incident shock wave, as it slid on the working surface of the devices. But later the waves reflected at the bunker wall and the ground loaded these gauges at different angles. The gauges placed on one side of supporting pipe are denoted hereafter by symbol “a”, and that placed on another side by “b”.

The time histories of pressure measured in the bunker after the detonation enable us to determine the characteristics of blast waves generated by layered charges. The overpressure history of a primary wave could usually be fitted by the modified Friedlander equation as follows [38].

$$P = P_s e^{-\alpha t} \left(1 - \frac{t}{\tau}\right) \quad (11)$$

where  $P$  is the overpressure at a gauge surface,  $P_s$  is the peak overpressure immediately behind the primary shock,  $t$  is the time after arrival of the primary shock at the gauge,  $\tau$  is the positive duration, and  $\alpha$  is a coefficient. The most important parameters of the blast wave are the pressure amplitude  $P_s$  and the pulse of the primary wave described by the equation:

$$I_s = \int_0^\tau \Delta p(t) dt \quad (12)$$

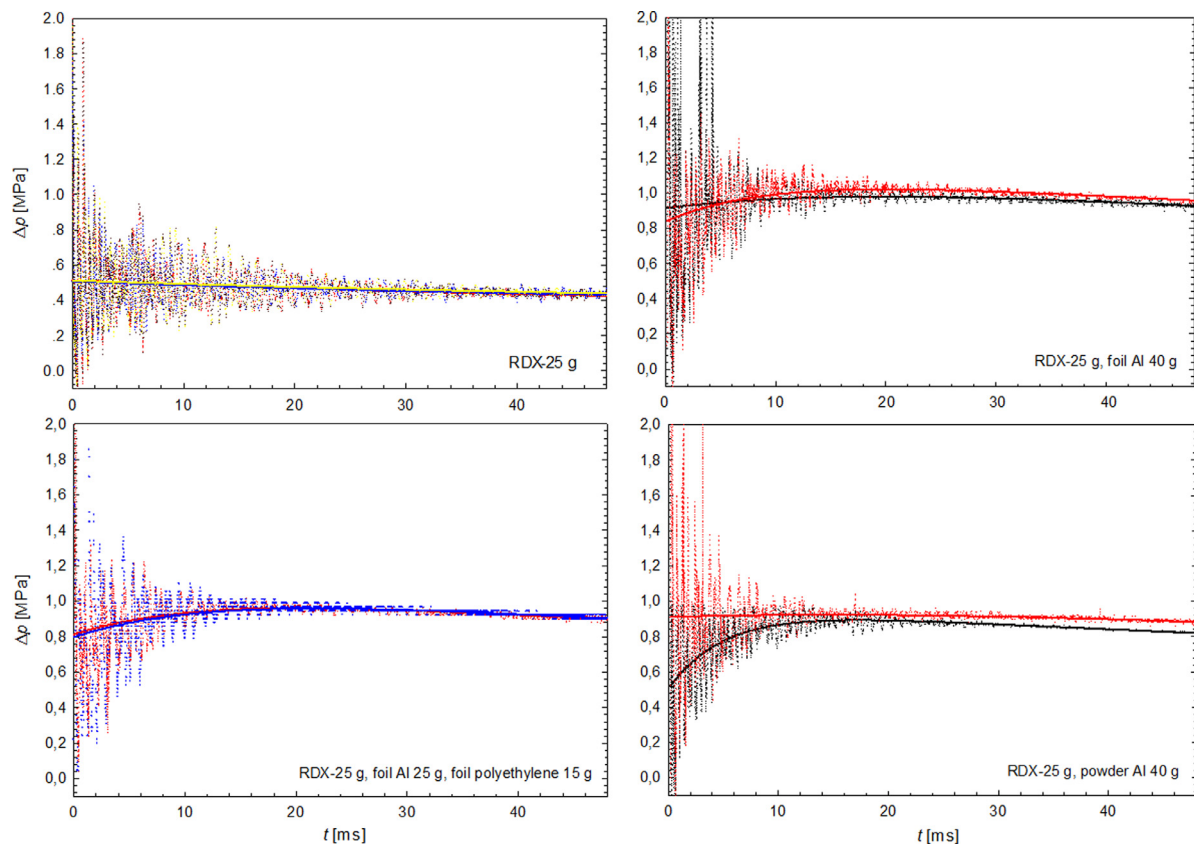


**Fig. 3.** Overpressure histories recorded in the 0.15 m<sup>3</sup> chamber after detonation of RDX<sub>ph</sub>, RDX<sub>ph</sub> + Al foil, RDX<sub>ph</sub> + Al/PE foils and RDX<sub>ph</sub> + Al powder charges (dots represents the experimental values and solid lines are fitting curves, while different color means repeated experiments). (For interpretation of the references to color in this figure legend, the reader is referred to the web version of this article).

If the overpressure change is described by the Friedlander equation, the value of the pulse  $I_s$  can be determined from the following equation:

$$I_s = \frac{P_s}{\alpha} \left( 1 - \frac{1 - e^{-\alpha\tau}}{\alpha\tau} \right) \quad (13)$$

The cylindrical charges used in the bunker had an explosive core with a diameter of 25.0 mm. It was composed of five pellets of RDX/wax 94/6 composition (RDX<sub>ph</sub>). The pellets had a density of 1.66 g cm<sup>-3</sup> and were glued together. RDX<sub>ph</sub> cores weighed 110.0 g. The external layer (envelope) included of Al<sub>f</sub>, Al<sub>p</sub> or a combination of Al and polyethylene foils (Al/PE). Additionally, one test with Al foil of thickness of 100 μm (Alf100) was performed in the bunker. The mass of external layer (envelope) was 136 g, and in the case of Al/PE layer, the foils were wound alternately and uniformly with mass ratio Al/PE = 85 g/51 g.

#### 2.4. Flame propagation obtained by high-speed camera

The fire-ball is considered to be one of the main features resulted from TBX action. The sustained fire-ball can have a lethal effect on fortified persons in caves and bunkers. High speed camera recorder was used to track the explosion events for the designed charges at 7500, 10,000 and 15,000 frames per second. Different snapshots at different time intervals were captured to determine the fire-ball duration, as well as its dimension changes. Using known lengths in the images recorded, based on image analysis (pixel vs. length correlation) an estimation of fire-ball dimensions was possible.

### 3. Results and discussions

#### 3.1. The QSP curves

Overpressure histories that were measured in the explosion chamber are shown in Figs. 3 and 4. Values of  $\Delta p_{\max}$  determined on the basis of at least two pressure histories are summarized in Table 2. The Table also provides values of overpressure  $\Delta p_{\text{cal}}$  calculated for the constant-volume explosion of the charges in the chamber with air (not taking into account of the heat loss to

**Table 2**

Values of  $\Delta p_{\max}$  obtained from the over-pressure histories measured in the chamber with air and calculated by using CHEETAH code.

Charge code	$\Delta p_{\max}$ [MPa]	Average $\Delta p_{\max}$ [MPa]	$\Delta p_{\text{cal}}$ [MPa]	$\frac{\Delta p_{\max}}{\Delta p_{\text{cal}}} \times 100\%$
RDX <sub>ph</sub>	0.514 0.508 0.512	0.51	0.60	85.0
RDX <sub>ph</sub> + Al foil (10 μm)	0.983 1.023	1.00	1.34	74.6
RDX <sub>ph</sub> + Al/PTFE foils	0.985 0.955 0.977 1.014	0.98	1.25	<b>78.4</b>
RDX <sub>ph</sub> + Al/Ni foils	0.802 0.760	0.78	–	–
RDX <sub>ph</sub> + Al/PE foils	0.962 0.960	0.96	1.44	66.7
RDX <sub>ph</sub> + Al powder	0.894 0.923	0.90	1.34	<b>67.2</b>

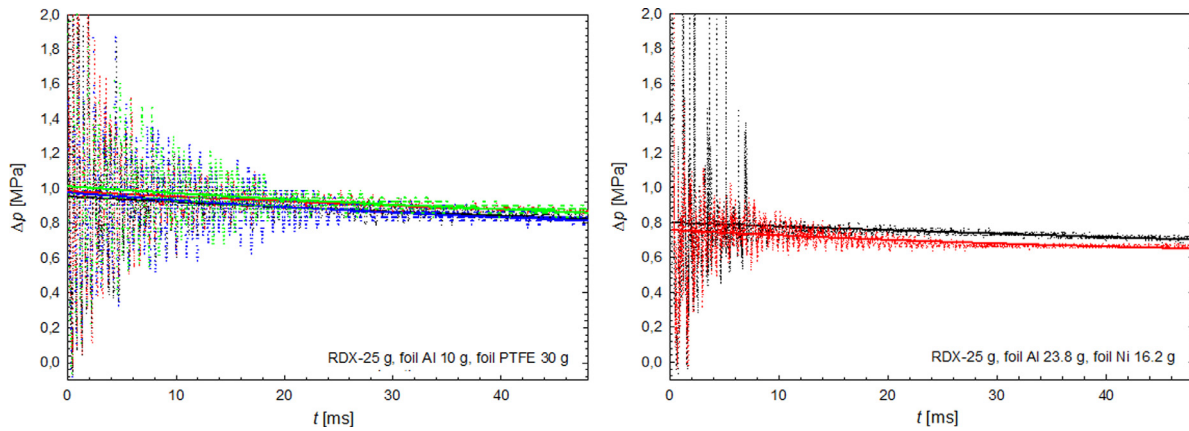


**Fig. 4.** Overpressure histories recorded in the 0.15 m<sup>3</sup> chamber after detonation of RDX<sub>ph</sub> + Al/PTFE foils and RDX<sub>ph</sub> + Al/Ni foils charges (dots represents the experimental values and solid lines are fitting curves, while different color means repeated experiments). (For interpretation of the references to color in this figure legend, the reader is referred to the web version of this article).

the wall of the chamber). Calculations were performed by using the CHEETAH code [26]. The main oscillations in the overpressure records are caused by shock wave reverberations at the chamber wall, while their amplitudes decrease with the time. There is also observed “noise” on pressure histories of smaller amplitude and higher frequency. These disturbances are the result of turbulence of gaseous medium, reverberations of shock waves inside the chamber sockets and vibration of the measuring system.

As shown in Fig. 3, the values of QSP for RDX<sub>ph</sub> with aluminized polymer films are higher than that of the pure RDX<sub>ph</sub>. The heat of reaction causes an increase of temperature and pressure of gaseous mixture in the chamber, indicating that Al reacts with oxygen from the air and oxidizing intermediates from detonation products. This conclusion is supported by the results of similar experiments with RDX<sub>ph</sub> + Ni/Al (mass ratio: 23.8/16.2) composition, in which the Ni film may behave like an inert additive, and hence the obtained QSP values for this charge are much lower than those of the RDX<sub>ph</sub> + Al charges. However, the QSP values of RDX<sub>ph</sub> + Ni/Al are still much higher than that of the pure RDX<sub>ph</sub> charge. The repeatability

of QSP for RDX<sub>ph</sub> charges with pure Al<sub>p</sub> or Al<sub>f</sub> was not as good as with aluminized polymer films. This result may be explained by a random failure of the ignition of Al<sub>p</sub> or fragmented Al<sub>f</sub>.

The data presented in Table 2 show that the use of the outer layer made of Al foils could increase the quasistatic pressure by as much as twice. However, the measured values of this pressure are much lower than the calculated average pressures in the chamber. Charges with Al foils out-layers produce higher values Δ*p*<sub>max</sub> than the charges containing Al<sub>p</sub> due to higher combustion efficiency of the foils, resulting in higher Δ*p*<sub>max</sub>/Δ*p*<sub>cal</sub>.

### 3.2. Pressure histories in a 40 m<sup>3</sup> bunker

The time histories of pressure measured in the 40 m<sup>3</sup> bunker after the detonation, enable us to determine the characteristics of blast waves generated by layered charges. The typical results of experimental overpressure data and corresponding fitted curves are shown in Figs. 5 and 6. The values of the overpressure peak

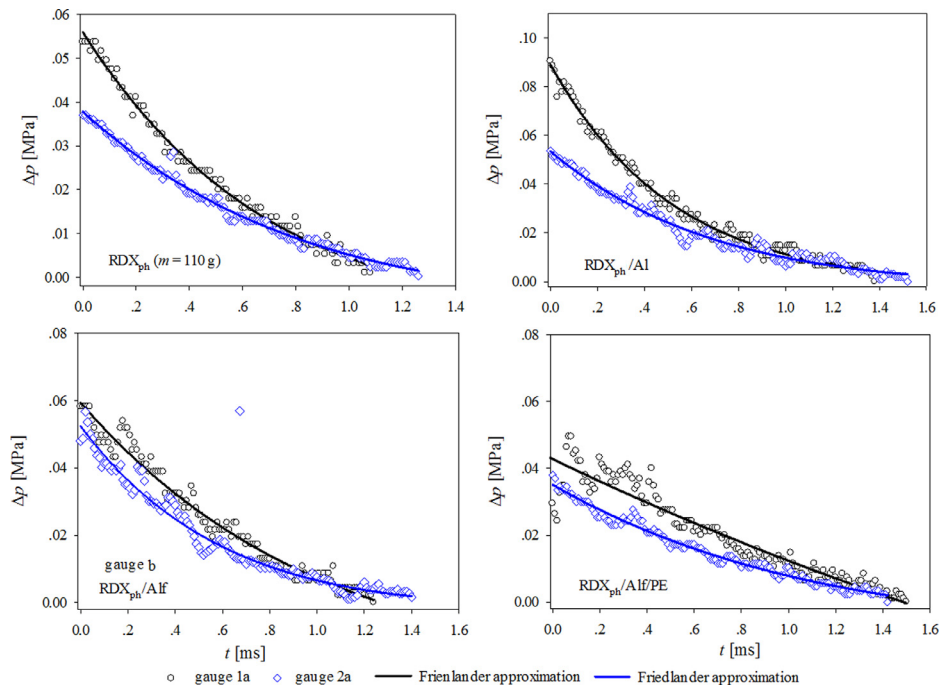


**Fig. 5.** Overpressure measured in the bunker after the explosion of the layered charges with Al foils of 10 (left) and 100 μm (right) thickness (the location of gauge No. 1 and No. 2 at distance of 2.0 m and 2.5 m, respectively, Fig. S1).

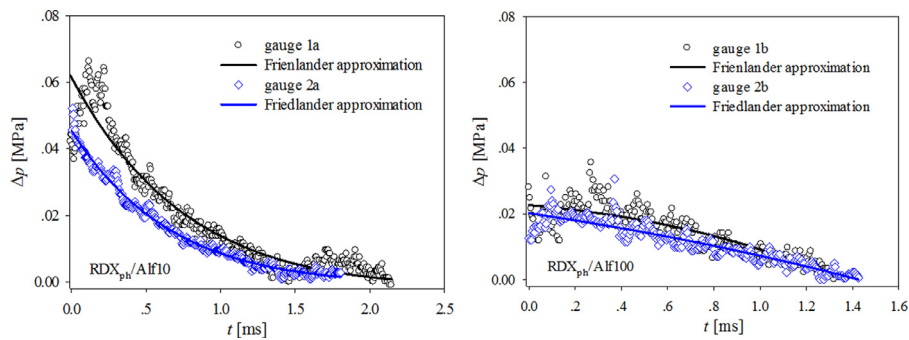


Fig. 6. Overpressure measured in the bunker after the explosion of the RDX<sub>ph</sub>, RDX<sub>ph</sub>/Alf10, RDX<sub>ph</sub>/Al<sub>p</sub>, and RDX<sub>ph</sub>/Alf-PE foils charges.

Table 3

Parameters of incident blast waves in the bunker at a distance of 2.0 and 2.5 m from the charge.

Charge symbol	Amplitude $P_s$ [kPa]		Specific impulse $I_s$ [Pa s]	
	At 2.0 m	At 2.5 m	At 2.0 m	At 2.5 m
RDX <sub>ph</sub> (core)	56	38	25	19
RDX <sub>ph</sub> + Al foil (10 μm)	60	–	35	–
	59	30	30	25
	62	45	40	26
	69	41	32	22
RDX <sub>ph</sub> + Al/PE foils	41	27	33	21
	43	35	31	22
	89	53	43	30
RDX <sub>ph</sub> + Al powder	–	44	–	32
	61	37	37	27
	64	44	32	24
	27	23	22	16
RDX <sub>ph</sub> + Al foil (100 μm)	28	20	19	16

and the specific impulse (obtained from the integration of the first peak) for an incident blast wave are listed in Table 3.

As shown in Figs. 5 and 6, the overpressure values obtained by gauge No. 1 are always larger than those obtained by the gauge No. 2, where the latter detects the overpressure waves at a longer distance with attenuation. The pressure amplitudes of RDX<sub>p</sub>/Alf-PE and RDX<sub>ph</sub>/Alf100 (with large fluctuations) are much lower than those of the other examined charges due to lower combustion efficiency, and they are even lower than that of the pure RDX<sub>ph</sub> charges. By comparing the performances of the charges containing Alf with different thickness (Fig. 5), it is clear that the charge with thinner Alf exhibits higher overpressure due to higher heat generation from more complete combustion of fragmented Alf. It also means that the thinner Alf may be transformed to Al fragments with smaller particle sizes, which are easier to be ignited. It can also be seen that the experimental time durations of pressure wave by the detonation gaseous products of tested aluminized explosives are longer than those measured for pure RDX<sub>ph</sub> charges, where the charge of RDX<sub>ph</sub>/Alf10 has the longest duration (better thermobaric performance).

As shown in Table 3, the amplitude and specific impulse of the blast waves at closer position to the charge are higher than those at far location, due to attenuation in the air. The tests of the amplitude for RDX<sub>ph</sub>/Alf10 and RDX<sub>ph</sub>/Al<sub>p</sub> charges has been repeated 4 times due to large discrepancies among individual tests, and the other curves are shown in Figs. S2 and S3 (Supporting information). The amplitude value of 89 kPa and specific impulse of 43 Pa s obtained at 2.0 m for RDX<sub>ph</sub>/Al<sub>p</sub> charges should be excluded due to a large error. It might be also the case for RDX<sub>ph</sub>/Alf10 showing pressure of 69 kPa and impulse of 40 Pa s at 2.0 m. When comparing the thermobaric effect from the small explosion chamber (0.15 m<sup>3</sup>) with that from the 40 m<sup>3</sup> bunker, one has to think about

Table 4

Total impulse in the bunker for  $t = 45$  ms at 2.0 and 2.5 m from the charge.

Charges	Total impulse $I$ [Pa s]		Charges	Total impulse $I$ [Pa s]	
	At 2.0 m	At 2.5 m		At 2.0 m	At 2.5 m
RDX <sub>ph</sub> /Alf (10 μm)	1020	740	RDX <sub>ph</sub> /Al <sub>p</sub>	1170	1031
	816	532		1130	1035
	1077	883		1171	904
RDX <sub>ph</sub> /Al-PE foils	–	529	RDX <sub>ph</sub> /Alf100	871	571
	814	681		487	374
	613	413		–	212
RDX <sub>ph</sub> (core)	368	366			

the contrasting reaction conditions encountered in the chamber and the bunker: the density of reactants in 0.15 m<sup>3</sup> detonation chamber is about 160 g m<sup>-3</sup>, while it is 2.75 g m<sup>-3</sup> for the larger bunker. Therefore, the first scenario is a near perfect stirred reactor with near perfect isochoric conditions (so-called quasi-static), the latter is a too small HE/volume ratio which counteracts the required intense reflected shockwave heating of the detonation products plume, resulting in underestimated thermobaric performances of our new concept.

### 3.3. The histories of the impulses

One of the important blast wave characteristics in semi-closed structures can be impulses determined for the specified time duration. The histories of the impulses calculated for a time period of 45 ms after the shock wave reached the gauges in the bunker are presented in Figs. 7 and 8. It is a measure of performance of the explosives tested (their capability to perform work).

In general, there are three stages for the thermobaric effect, which are initial stage, anaerobic stage, and aerobic stage. As mentioned in the introduction part, the metal and the detonation product react with oxygen from condensed air (shock wave front). Due to a large density gradient, the R-T (Rayleigh–Taylor) instability turbulent flow can be used to explain this mixing and burning step [39,40]. The shock wave reflected by the wall of the airtight environment reacts with the high speed fireball generated by the above-mentioned process. The turbulent flow burning [41–43] is increased and the boundary temperature of the fireball rises to reignite the mixture of the metal and the detonation products. Blast waves are intensified when reflected by walls and other surfaces, which is the reason of the multi peaks generated at different times (Figs. 7 and 8). Moreover, the charges enveloped by Alf have larger peak values of overpressure (about 0.25 MPa) than those of RDX<sub>ph</sub> core and RDX<sub>ph</sub>/Al<sub>p</sub> (< 0.20 MPa), indicating that the Alf can generate a better blast performance than the Al<sub>p</sub>. The total impulses determined for time duration of 45 ms, produced by all the tested charges are summarized in Table 4.

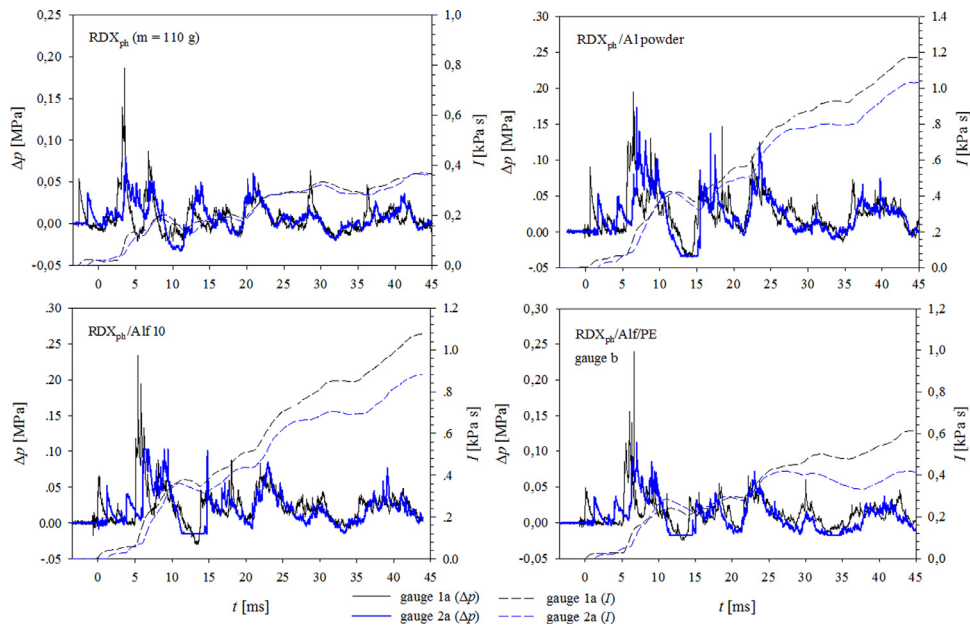


Fig. 7. Pressure and impulse histories at a distance 2.0 and 2.5 m for  $\text{RDX}_{\text{ph}}$ ,  $\text{RDX}_{\text{ph}}/\text{Al}_p$ ,  $\text{RDX}_{\text{ph}}/\text{Alf}10$ , and  $\text{RDX}_{\text{ph}}/\text{Al-PE}$  foils charges.

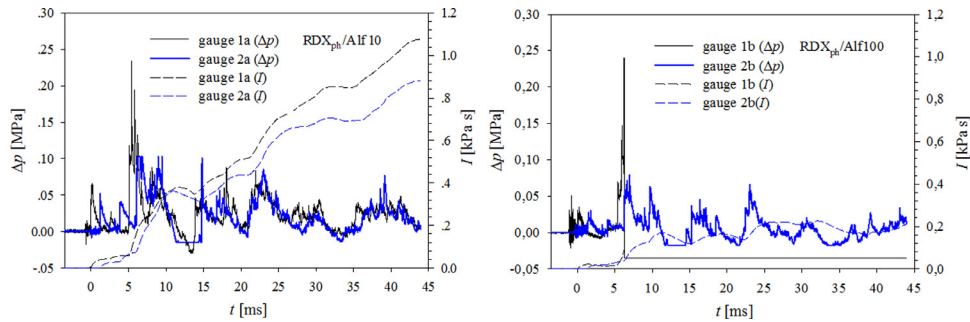


Fig. 8. Pressure and impulse histories at a distance 2.0 and 2.5 m for  $\text{RDX}_{\text{ph}}/\text{Alf}$  (10 and 100  $\mu\text{m}$  thickness).

From the data shown in Table 4, it is clear that the total impulses at a distance of 2.0 m for enveloped charges containing Alf and  $\text{Al}_p$  are almost three times higher than that of simple  $\text{RDX}_{\text{ph}}$  charge. In the semi-closed bunker, charges containing  $\text{Al}_p$  performs slightly better than those with thin Al foil. It may be caused by incomplete combustion, as very fine unburned fragments of the 100  $\mu\text{m}$  thickness foil were found in the bunker after detonation of  $\text{RDX}_{\text{ph}}/\text{Alf}100$  charges (Fig. S8).

Under the conditions of larger volume, practically an open space for so small charges, aluminized PE foil behaves like an inert material. It was found previously that there is a clear growing trend in impulses with increasing Al content in an outer envelope [20]. The highest values of the impulse, obtained for layered charges containing only  $\text{Al}_p$ , is about 1170 Pa s at a distance of 2.0 m. If we compare overpressure results obtained from 0.15  $\text{m}^3$  chamber and 40  $\text{m}^3$  bunker, we could notice that the reflected shock waves are stronger in the small bunker due to the shorter distance between the charge and the wall. This creates more effective heating of the reactive mixture inside the chamber, resulting in better combustion efficiency.

### 3.4. Simultaneous fragmentation and ignition

Considering the Grady model, the metallic envelope fragmentation can be seen as a natural fragmentation process with some degree of heterogeneity [28]. In order to evaluate the charac-

Table 5

Calculated results for 1 foil and 1D fragmenting approach.

Model parameter	Mott	Grady	Goloveshkin and Myakov	
			10 $\mu\text{m}$ thickness	100 $\mu\text{m}$ thickness
Characteristic length (mm)	0.094	1.116	0.394	0.848
Number of fragments	832	70	199	93

teristic length of fragments for the case of  $\text{RDX}/\text{Alf}$  configuration, two assumptions have been made: the fragments will retain the inner and outer surface of the original shell, due to the extremely small thickness (10  $\mu\text{m}$  or 100  $\mu\text{m}$ ) and each layer of Al foil will behave exactly the same. Based on the above assumptions, a 1D approach was utilized since both circumferential dimension and height of the Al foil are in similar range. For the Al foil an AA1100-0 material was adopted, whose mechanical characteristics are available in the literature and has manufacture specifications of density (2.71  $\text{g cm}^{-3}$ ), Young modulus (68.9 GPa), yield stress (34.5 MPa), fracture stress (89.6 MPa), fracture strain (0.15), dynamic fracture toughness (25  $\text{MPa m}^{1/2}$ ) and proportionality coefficient ( $P_2 = 372 \text{ MPa}$ ). Using Gurney expression for an axial symmetric configuration, an average value of  $1.7 \times 10^5 \text{ s}^{-1}$  (referring to all Al layers) for the considered strain rates. The results obtained for the proposed models are summarized in Table 5.

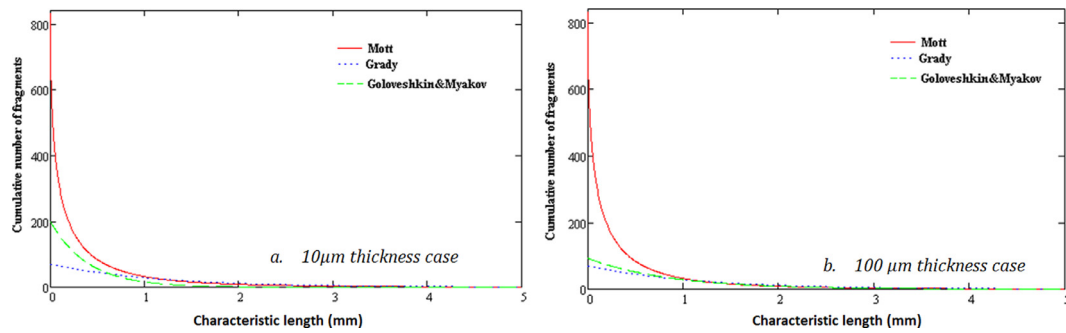


Fig. 9. Cumulative distribution of fragments characteristic diameter.

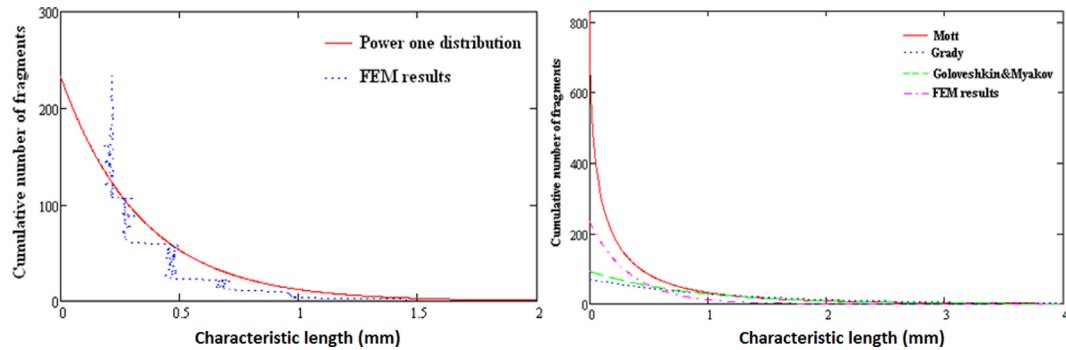


Fig. 10. FEM simulation results and Analytical vs FEM results for AlF100 case.

The statistical cumulative distributions for the fragments in terms of characteristic length based on Eqs. (4), (7) and (10) are depicted in Fig. 9.

As an alternative to the previously-presented analytical method, a numerical simulation using LsDyna software was also used. The defined 2D simulation (Fig. S6) refers to a single layer of Al foil. The used mesh had one element of thickness, one element of height and a size of  $100\ \mu\text{m}$  in circumferential direction. For the 0.15 Al fracture strain value an almost centered Weibull distribution with a value of 5 for the scale parameter (corresponding to a 5% variation of the nominal failure strain value) was considered. Similar approach was described in detail by Fagerholt [44], Watson [45] and Trană [46]. The results obtained by the simulations indicate formation of about 233 fragments with an average characteristic length of 0.337 mm. In comparison, by using a post-processing algorithm regarding the fragment analysis, the number of fragments and their characteristic length were determined and depicted in Fig. 10a. Also, in the same figure a power one cumulative distribution is super-imposed since such a distribution fairly agrees with the numerical findings.

Analyzing the results provided by the presented analytical methods, one can observe that Mott method indicates by far the highest number of fragments as compared with the other two methods. This discrepancy could also be resulted from the high value of the strain rate assumed in the calculus [47]. The fragmentation process is usually governed fully by the flaw structure, but at high nucleation rates, the process is determined strictly by the fracture energy resisting fracture growth. With respect to Goloveshkin and Myakov method, the results clearly indicate that when the wall thickness is increased, the obtained values are close to the values that are calculated by Grady method. By comparing the two sets of results (analytical and fragmentation experimental measurement, FEM), it could be seen that there is a good correlation between them (Fig. 10b). However, as a common observation for all four examined models, it can be concluded that the calculated fragment characteristic length is several times higher than

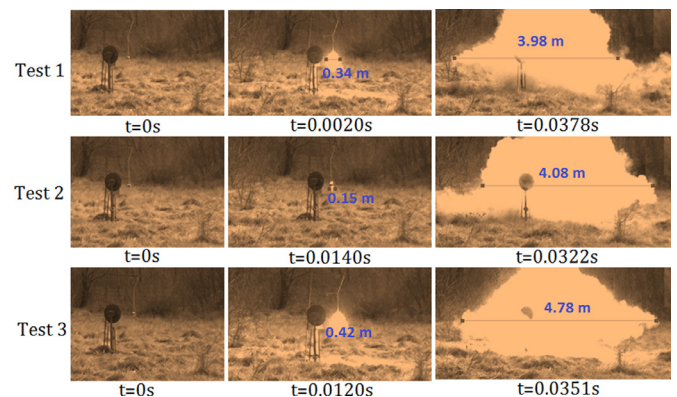


Fig. 11. Flame propagation after explosion of RDX core charges enveloped by AlF10 in the open field obtained by a high-speed camera (3 repeating tests).

the AlF thickness. This can lead to a justification that the observed blast enhancement is dependent not on the thickness but on the surrounding space. This observation is also strongly supported by the fact that for the  $100\ \mu\text{m}$  Al foil, the bunker tests indicated a blast enhancement and several unburnt foil fragments were retrieved after tests (Fig. S8), while for open field tests, according to high speed camera images, most of the Al fragments are ejected and ignited (Fig. S9).

### 3.5. The flame propagation and sizes of fire-balls

In this study image analysis was employed to quantify the fire-ball size, as well as its characteristic features with time. The set of images captured by the high speed camera was processed, each image being transferred to a binary image. Typical images from open field tests are presented in Fig. 11.

It could be seen that the fire-ball was growing up quickly and turned into mushroom shape (characteristic feature of thermobaric

action) at around 35 ms after the initiation of RDX<sub>ph</sub> core charge. The fire-ball exhibited a sustained effective action up to 40 ms and the extended action of fire-ball is one of the main TBX characteristics as well. In general, the fire-ball exhibited effectiveness over the time delay from 10 to 40 ms. Our novel designed layered charges could be considered as more effective TBX than presently used normal TBX charges containing Al powder, which usually sustain the fire-ball of less than 40 ms. In terms of the sizes, the fire-ball generated by our layered charges could reach the radius of about 2.4 m from the center of its detonation point.

#### 4. Conclusions

The detonation experiments performed in bunkers and open fields showed that the strong thermobaric effects could be generated by the layered charges with novel designs. This design allows to overcome many technical issues related to production of TBX charges using micron- or nano-sized Al particles. Our design is based on simultaneous fragmentation and ignition of simple Al foils enveloping cylindrical charges or charged with other shapes. Also, the fragmentation processes of Alf have been simulated by Mott and Grady models and compared with the experimental results. The following conclusions were made:

- (1) The values of QSP for RDX<sub>ph</sub> enveloped with Alf are higher than that of the pure RDX<sub>ph</sub> due to increase of temperature by heat generation from the foil combustion. The quasi-static pressure generated by RDX<sub>ph</sub>/Al–Ni foils charge is much lower than those of the RDX<sub>ph</sub>/Alf charges due to relatively inert nature of Ni.
- (2) In a small chamber, the RDX<sub>ph</sub>/Alf charges produce even higher  $\Delta p_{\max}$  values than the charges containing Al<sub>p</sub> due to higher combustion efficiency. In a 40 m<sup>3</sup> bunker, the impulse amplitudes of RDX<sub>ph</sub>/Al–PE foils and RDX<sub>ph</sub>/Alf100 charges were found to be much lower than those of the other charges due to less combustion efficiency, and they are even lower than that of the pure RDX<sub>ph</sub> charge.
- (3) The charges enveloped by Al foils have larger overpressure peak values (about 0.25 MPa) than those of RDX<sub>ph</sub> core and RDX<sub>ph</sub>/Al<sub>p</sub> charges (<0.20 MPa), meaning that the Alf generates better blast performances than the Al particles.
- (4) The simulations indicate that 233 fragments with an average characteristic length of 0.337 mm have been generated, which is several times larger than the thickness of Alf, indicating that the blast enhancement is dependent more on the surrounding space than on the thickness of the foil.
- (5) The fire-ball with thermobaric feature generated by combustion of Alf grew up quickly and turned into mushroom shape after about 35 ms from the initiation of RDX core charge. Such fire-ball could sustain combustion up to 40 ms, reaching a radius of about 2.4 m. The observed performances of our new thermobaric charges showed the significant advantages of previously known designs.

#### Acknowledgment

This work has been financially supported by the Tel Aviv University (Israel), Military University of Technology (Warsaw, Poland), and Military Technical Academy (Bucharest, Romania).

#### Supplementary materials

Supplementary material associated with this article can be found, in the online version, at [doi:10.1016/j.combustflame.2016.01.010](https://doi.org/10.1016/j.combustflame.2016.01.010).

#### References

- [1] X.L. Xing, S.X. Zhao, Z.Y. Wang, G.T. Ge, Discussions on thermobaric explosives (TBXs), *Propellants Explos. Pyrotech.* 39 (2014) 14–17.
- [2] K.M. Jaansalu, M.R. Dunning, W.S. Andrews, Fragment velocities from thermobaric explosives in metal cylinders, *Propellants Explos. Pyrotech.* 32 (2007) 80.
- [3] W.A. Trzcinski, L. Maiz, Thermobaric and enhanced blast explosives – properties and testing methods, *Propellants Explos. Pyrotech.* 40 (5) (2015) 632–644.
- [4] G. Neuneck, The revolution in military affairs: its driving forces, elements, and complexity, *Complexity* 14 (2008) 50.
- [5] A.E. Wildegger-Gaissmaier, Aspects of thermobaric weaponry, *ADF Health* 4 (2003) 3.
- [6] N.H. Yen, L.Y. Wang, Reactive metals in explosives, *Propellants Explos. Pyrotech.* 37 (2012) 143–155.
- [7] R.L. Geisler, A global view of the use of Al fuel in solid rocket motors, 38th AIAA/ASME/ASE/ASEE Joint Propulsion Conference and Exhibit, Indianapolis, IN, USA, July 7–10, 2002 AIAA 2002-3748.
- [8] R.A. Yetter, G.A. Risha, S.F. Son, Metal particle combustion and nanotechnology, *Proc. Combust. Inst.* 32 (2009) 1819–1838.
- [9] A.K. Mohamed, H.E. Mostafa, S. Elbasuney, Nanoscopic fuel-rich thermobaric formulations: chemical composition optimization and sustained secondary combustion shock wave modulation, *J. Hazard. Mater.* (2015), doi:10.1016/j.jhazmat.2015.09.019.
- [10] J. McCollum, M.L. Pantoya, S.T. Iacono, Activating Al reactivity with fluoropolymer coatings for improved energetic composite combustion, *ACS Appl. Mater. Interfaces* 7 (2015) 18742–18749.
- [11] S.C. Kettwich, K. Kappagantula, B.S. Kusel, E.K. Avjian, S.T. Danielson, H.A. Miller, M.L. Pantoya, S.T. Iacono, Thermal investigations of nanoAl/perfluoropolyether core-shell impregnated composites for structural energetics, *Thermochim. Acta* 591 (2014) 45–50.
- [12] T.R. Sippel, S.F. Son, L.J. Groven, Altering reactivity of Al with selective inclusion of polytetrafluoroethylene through mechanical activation, *Propellants Explos. Pyrotech.* 38 (2013) 286–295.
- [13] H.A. Miller, B.S. Kusel, S.T. Danielson, J.W. Neat, E.K. Avjian, S.N. Pierson, S.M. Budy, D.W. Ball, S.T. Iacono, S.C. Kettwich, Metastable nanostructured metallized fluoropolymer composites for energetics, *J. Mater. Chem. A* 1 (24) (2013) 7050.
- [14] K.S. Kappagantula, C. Farley, M.L. Pantoya, J. Horn, Tuning energetic material reactivity using surface functionalization of Al fuels, *J. Phys. Chem. C* 116 (46) (2012) 24469–24475.
- [15] E.-C. Koch, Metal-fluorocarbon based energetic materials, Wiley-VCH, Weinheim, Germany, 2012.
- [16] J.D.E. White, R.V. Reeves, S.F. Son, A.S. Mukasyan, Thermal explosion in Al–Ni system: influence of mechanical activation, *J. Phys. Chem. A* 113 (2009) 13541–13547.
- [17] D.A. Reese, L.J. Groven, S.F. Son, A.S. Mukasyan, Intermetallic compounds as fuels for composite rocket propellants, 47th AIAA/ASME/ASE/ASEE Joint Propulsion Conference and Exhibit, 2011 AIAA 2011-5865.
- [18] M.L. Chan, G.W. Meyers, Advanced thermobaric explosive compositions. Patent US 6,955,732 B1, 2005.
- [19] M.L. Chan, D.T. Bui, G. Meyers, A. Turner, Castable thermobaric explosive formulations. Patent US 6,969,434 B1, 2005.
- [20] W.A. Trzcinski, S. Cudziło, L. Szymanczyk, Studies of detonation characteristics of aluminium enriched RDX compositions, *Propellants Explos. Pyrotech.* 32 (2007) 392–400.
- [21] J. Paszula, W.A. Trzcinski, K. Sprzaczak, Detonation performance of aluminium–ammonium nitrate explosives, *Cent. Eur. J. Energetic Mater.* 5 (1) (2008) 3–12.
- [22] W.A. Trzcinski, K. Barcz, Investigation of blast wave characteristics for layered thermobaric charges, 21st International Symposium on Military Aspects of Blast and Shock, 2010 97–91.
- [23] W.A. Trzcinski, K. Barcz, Investigation of blast wave characteristics for layered thermobaric charges, *Shock Waves* 22 (2012) 119.
- [24] W.A. Trzcinski, K. Barcz, J. Paszula, S. Cudziło, Investigation of blast performance and solid residues for layered thermobaric charges, *Propellants Explos. Pyrotech.* 39 (2014) 40–50.
- [25] F. Zhang, L. Donahue, W.H. Wilson, The effect of charge reactive metal cases on air blast, 16th APS Topical Conference on Shock Compression of Condensed Matter, June 28–July 3, American Physical Society, 2009.
- [26] L.E. Fried, Cheetah 1.39 – user's manual, LLNL, 1996.
- [27] N.F. Mott, Fragmentation of shell cases, *Proc. R. Soc. Lond. Ser. A (Math. Phys. Sci.)* 189 (1947) 300–308.
- [28] D.E. Grady, Length scales and size distributions in dynamic fragmentation, *Int. J. Fract.* 163 (2010) 85–99.
- [29] A. Rotariu, E. Trană, C. Dima, C. Enache, F. Timplaru, L. Matache, Uninstrumented measurement method for granular porous media blast mitigation assessment, *Exp. Tech.* (2015), doi:10.1111/ext.12155.
- [30] P. Rosin, E. Rammler, The laws governing the fineness of powered coal, *J. Inst. Fuel* 7 (1933) 29–36.
- [31] C.C. Lienau, Random fracture for brittle solid, *J. Frankl. Inst.* 221 (1936) 485–494.
- [32] W. Weibull, A statistical theory of strength of materials, Ingeniors Vetenskapssakad, 151, Generalstabens litografiska anstalts förlag, 1939.
- [33] E.V. Schuhmann, Principles of communication, size distribution and surface calculation, vol. 1189, AIME Technical Publication, 1941, pp. 1–11.

- [34] J.J. Gilvary, Fracture of brittle solids: 1. Distribution function for fragment size in single fracture (theoretical), *J. Appl. Phys.* 32 (1961) 391–399.
- [35] D.A. Shockey, D.R. Curran, L. Seaman, C.F. Petersen, Fragmentation of rock under dynamic loads, *Int. J. Rock Mech. Geomech. Abstr.* 11 (1974) 303–317.
- [36] F. Zhang, J. Anderson, A. Yoshinaka, Post detonation energy release from TNT-Al explosives, *Shock Compression of Condensed Matter, American Institute of Physics*, 2007, pp. 885–888.
- [37] V.A. Goloveshkin, N.N. Myagkov, Fragmentation model for expanding cylinder, *Int. J. Fract.* 187 (2014) 239–243.
- [38] J.M. Dewey, The shape of the blast wave: studies of the Friedlander equation, *International Symposium on Military Aspects of Blast and Shock*, 2010.
- [39] S.I. Anisimov, Y.B. Zel'dovich, Rayleigh–Taylor instability of the boundary between detonation products and gas in a spherical explosion, *Pis'ma Zh. Eksp. Teor. Fiz.* 3 (1977) 1081.
- [40] S.I. Anisimov, Y.B. Zel'dovich, M.A. Inogamov, M.F. Ivanov, The Taylor instability of contact boundary between expanding detonation products and a surrounding gas, *Shock waves, explosions, and detonations (A84-28376 12-34)*, American Institute of Aeronautics and Astronautics, Inc., New York, 1983, pp. 218–227.
- [41] P. Wolanski, Z. Gut, W.A. Trzcinski, L. Szymanczyk, J. Paszula, Visualization of turbulent combustion of TNT detonation products in steel vessel, *Shock Waves* 10 (2000) 127.
- [42] R. Hibert, F. Tap, H.E. Rabii, D. Thøvenin, Impact of detailed chemistry and transport models on turbulent combustion simulations, *Prog. Energy Combust. Sci.* 30 (2004) 61.
- [43] M.F. Gogulya, M.N. Makhov, A. Yu. Dolgoborodov, M.A. Brazhnikov, V.I. Arkhipov, V.G. Shchetinin, Mechanical sensitivity and detonation parameters of aluminized explosives, *Combust. Explos. Shock Waves* 40 (2004) 445.
- [44] E. Fagerholt, C. Dørum, T. Børvik, H.I. Laukli, O.S. Hopperstad, Experimental and numerical investigation of fracture in a cast aluminium alloy, *Int. J. Solids Struct.* 47 (24) (2010) 3352–3365.
- [45] R. Watson, W.D. Griffiths, T. Yeguer, S. Ruffe, Towards location specific statistical fracture prediction in high pressure die castings, *10th European LS-DYNA Conference 2015, Germany*, 2015.
- [46] E. Trană, A. Rotariu, F. Bucur, Numerical simulation study on the ring fragmentation, *MTA Rev.* 2 (XXV) (2015) 179–188.
- [47] D. Grady, Investigation of explosively driven fragmentation of metals—two-dimensional fracture and fragmentation of metal shells: progress report II, ARA Project No. 0950, 2003.